Molecular Mechanics Studies of Factors Affecting Overall Rate in Cascade Reactions: Multi-enzyme Colocalization and Environment

Shivansh Kaushik, Ta I Hung, Chia-en A. Chang\*

Department of Chemistry, University of California Riverside, Riverside, CA, USA, 92521

Keywords: multienzyme nanostructures, molecular modeling, molecular recognition, GeomBD3, enzyme-substrate binding, substate channeling.

## **ABSTRACT**

Millions of years of evolution have optimized many biosynthetic pathways by use of multi-step catalysis. In addition, multi-step metabolic pathways are commonly found in and on membranebound organelles in eukaryotic biochemistry. The fundamental mechanisms that facilitate these reaction processes provide strategies to bioengineer metabolic pathways in synthetic chemistry. Using Brownian dynamics simulations, here we modeled intermediate substrate transportation of colocalized yeast-ester biosynthesis enzymes on the membrane. The substrate acetate ion traveled from the pocket of aldehyde dehydrogenase to its target enzyme acetyl-CoA synthetase, then the substrate acetyl CoA diffused from Acs1 to the active site of the next enzyme, alcohol-Oacetyltransferase. Arranging two enzymes with the smallest inter-enzyme distance of 60 Å had the fastest average substrate association time as compared with anchoring enzymes with larger interenzyme distances. When the off-target side reactions were turned on, most substrates were lost, which suggests that native localization is necessary for efficient final product synthesis. We also evaluated the effects from intermolecular interactions, local substrate concentrations, and membrane environment to bring mechanistic insights into the colocalization pathways. The computation work demonstrates that creating spatially organized multi-enzymes on membranes can be an effective strategy to increase final product synthesis in bioengineering systems.

#### INTRODUCTION

In cells, the multistep reactions of cellular metabolism commonly involve multienzyme biosynthesis, the chemical process performed by several enzymes to produce a final product<sup>1,2</sup>. To study these reaction processes, in vitro experiments test cascade-mimicking reaction pathways or configurations involved in the multienzyme biosynthesis inside a biological system<sup>3-5</sup>. Most of the multienzyme cascades feature colocalized multistep reaction pathways to achieve maximum yield and minimize interferences by reducing byproducts or side reactions. Inside a living cell, natural phenomena such as compartmentalization and metabolic channeling create a spatial organization of enzymes for high yield and specificity. Multienzyme complexes found in nature include but are not limited to tryptophan synthase, polyketide synthase, the family of 2-oxoacid dehydrogenase complexes such as the pyruvate dehydrogenase complex, the ketoglutarate dehydrogenase complex, and cellulosomes<sup>6-12</sup>.

In addition to assembling multiple enzymes into an enzyme complex, colocalizing several enzymes on a membrane is also a strategy in biology. For example, *E. coli* colocalizes enzymes on the membrane to increase mevalonate, glucaric acid, and butyrate biosynthesis by 77-, 5-, and 3-fold, respectively<sup>13-15</sup>. With such spatial organization of enzymes, the local concentration and dwelling of substrate around binding pockets is increased, yielding enhanced enzyme efficiency<sup>16-18</sup>. The exploration of such spatially organized systems leads to a better understanding of mechanisms behind enzyme complexes and can lead to engineering in vitro enzymatic systems with effective synthetic pathways.

Many experiments have been designed to enhance enzymatic efficiency by anchoring enzymes to various molecular scaffolds and constructing spatially organized pathways<sup>19, 20</sup>. Although these efforts led to optimized synthetic multi-enzyme pathways, the detailed molecular mechanisms resulting in overall catalytic rate enhancement are not fully understood. Various factors may affect the productivity and rate of a final product synthesis during a multi-enzyme biosynthetic cascade by enzyme colocalization. For example, forming a multi-enzyme complex or even bringing enzymes together may allow for shorter traveling time and easier accessibility for a substrate to reach the active site of each enzyme to increase substrate association time and rate. Changes in protein dynamics when proteins are assembled may alter product synthesis<sup>21, 22</sup>. A multi-enzyme complex may even form a hydrophobic tunnel to keep a non-polar intermediate substrate<sup>23</sup> or a

polar channel to guide substrate transportation via electrostatic steering<sup>24, 25</sup>. Enhancing local substrate concentration by providing non-specific but favorable interactions to attract a substrate to proximity of the target enzyme can increase the final product synthesis rates as well.

Studying multi-enzyme cascades experimentally in a cell environment can be challenging. The effects of local environments and substrate concentrations affecting diffusion pathways of molecules to achieve catalysis are not directly observable with experimental measurements. Computational modeling has emerged as a powerful and less expensive tool to study many biological systems. All-atom molecular dynamics (MD) simulations are helpful in providing a better picture of binding events by considering all atoms in an explicit solvent model<sup>26-28</sup>. However, the size of the system and the computational cost to study them limit the use of MD simulations. Therefore, to model molecular encounters for large-scale systems, numerical methods and Brownian dynamics (BD) simulations have been used for several decades<sup>29, 30</sup>. For example, using the GeomBD3 program, developed to precisely handle biomolecular systems with specific environments and enzyme arrangements, simulations have been used to explore the spatially organized macroscopic systems to quantify and explain the effects on increased overall catalytic rates<sup>31-34</sup>. Theories have been established to numerically model molecular encounters or to compare the kinetics of enzyme complexes that catalyze multi-substrate reactions<sup>25, 35-39</sup>.

The Wheeldon group engineered an enzyme colocalization scaffold of yeast-ester biosynthesis on intracellular lipid droplets, mimicking the biosynthesis process in *Saccharomyces cerevisiae*. The group demonstrated a 2-fold increase in ethyl-acetate production by colocalizing the 3 enzymes: aldehyde dehydrogenase (Ald6), acetyl-CoA synthetase (Acs1) and alcohol-O-acetyltransferase (Atf1)<sup>40</sup>. As illustrated in **Figure 1D**, Ald6, Acs1, and Atf1 produce acetate ion (ACT), acetyl-CoA (ACO) and ethyl acetate, respectively. This metabolic pathway has 2 key intermediate transportation steps: diffusion of the product of Ald6, ACT, to Acs1 (Step 1 in **Figure 1E**) and the product of Acs1, ACO, to Atf1 (Step 2 in **Figure 1E**). The reaction mechanism of Acs1 to produce ACO can be simplified as follows:

Acs1 + acetate + ATP 
$$\longleftrightarrow$$
 Acs1.acetyl-AMP + PP<sub>i</sub>  
Acs1.acetyl-AMP + HSCoA  $\longleftrightarrow$  Acs1-AMP + acetyl-CoA

In the mechanism, an Acs1-bound acetyl-AMP intermediate (Acs1.acetyl-AMP) and pyrophosphate (PP<sub>i</sub>) are formed. Subsequently, the acetyl group of the intermediate reacts with the sulfhydryl group of coenzyme A (HSCoA) to produce ACO.

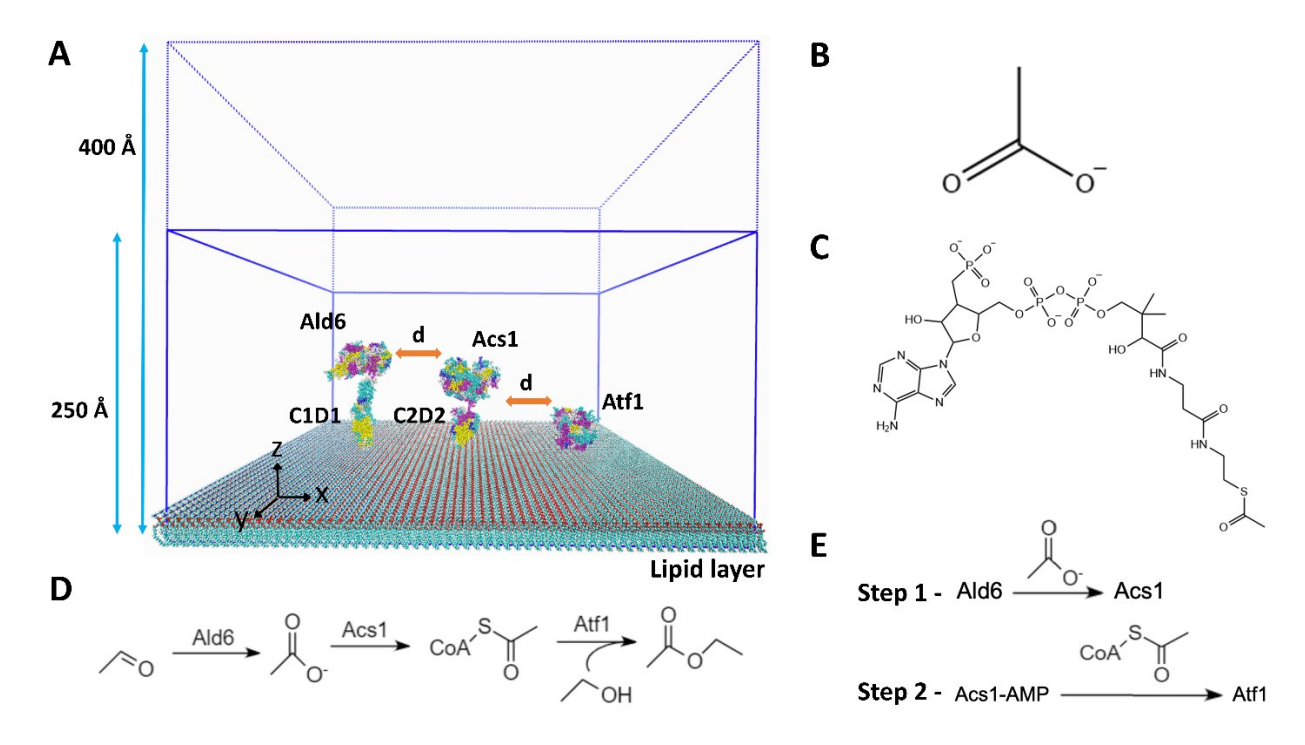


**Figure 1. System overview of multienzyme cascade reaction. (A)** Model System: Three enzymes (Ald6, Acs1 and Atf1) and 2 cohesin-dockerin molecules (C1D1 and C2D2) are placed on the lipid monolayer surface. The size of the simulation box for the test-tube environment is represented by a solid blue line (420 x 420 x 250 Å), and it extends up to 400 Å in the z-dimension, as indicated by the dotted line for the cell-like environment. The distance between the enzymes, represented by d, can be 60, 80, 100, or 500 Å. **(B)** Structure of acetate ion (ACT) and **(C)** acetyl CoA ligand (ACO). **(D)** Three-step yeast-ester biosynthesis mechanism in *Saccharomyces cerevisiae*. **(E)** Step 1 of the modeled reaction: acetate ion leaving Ald6 to bind Acs1 and form acetyl CoA. Step 2: acetyl CoA leaving Acs1 to bind Atf1 and form ethyl acetate.

To further understand how colocalization increases the final product synthesis, we used the GeomBD3 program to examine this yeast-ester biosynthesis system in atomistic-level detail (Figure 1A). As in the experimental setting, upstream enzymes Ald6 and Acs1 were placed on a lipid monolayer surface using cohesin-dockerin (C1D1 and C2D2) anchors, respectively, to localize the enzymes in the proximity of Atf1. Note that in the second step, our study used the Acs1-AMP complex instead of Acs1 to model ACO leaving the active site of the Acs1-AMP complex enzyme and then associating with the Atf1 enzyme. The colocalization effect was

introduced in the systems by placing the enzymes at different distances from each other. Our models considered 2 environments: a test-tube environment as a closed system and a cell-like environment with reaction side effects. We measured the association time of ACT and ACO with Acs1 and Atf1, respectively, and quantified and discuss mechanisms that affect distance-dependence associations such as intermolecular interactions, increased local concentrations, and proximity effects.

## **METHODS**

The setup of the modeling work is similar to the experiments carried out by the Wheeldon group, in which the three key enzymes — Ald6, Acs1, and Atf1 — were placed on lipid droplet membranes <sup>40</sup>. Two separate models were designed to simulate the diffusion of ACT from Ald6 to Acs1 for Step 1 and ACO from Acs1 to Atf1 for Step 2 (**Figure 1E**). Thereafter, we investigated the impact of colocalization by varying the inter-enzyme distances under different environments on the diffusion pattern and association kinetics of both substrates.

# Molecular models and force field parameters

Because no experimentally determined structures were available for Ald6 and Atf1 enzymes, we used homology modeling with the SWISS-MODEL tool to generate the modeled structures<sup>41</sup>. Sequence information from the Genome Database (YPL061W) and GenBank (NP\_015022.3), along with template structures (PDB IDs: 6TGW and 3FP0) exhibiting sequence similarities of 26% and 43%, respectively, was utilized for modeling the enzymes Ald6 and Atf1, respectively<sup>42</sup>. Both template structures have bound ligand. The binding site of PDB- 3FP0 was used as the Atf1 binding site. The setup and parameters of modeled Ald6, Acs1 (PDB ID: 1RY2) and modeled Atf1 were prepared with AMBER tleap using the Amber ff14SB force field<sup>44, 45</sup>. We used a 200-ns accelerated MD (aMD) simulation with 1 level of alpha potential on the Atf1 enzyme structure to analyze its binding pocket for the substrate to enter<sup>46</sup>. Selecting the appropriate protein conformation is crucial in BD simulations to accurately model substrate binding and unbinding events via accessible pathway. We chose an open-loop conformation from a 200ns aMD run, specifically at the 169 ns frame, due to its accessibility to the substrate, unlike the closed-loop conformation of the initial Atf1 structure (**Figure 2A** and **Figure S1**). This open conformation was

identified from a time frame with stable backbone RMSD, and we defined the binding site of 13.5 Šradius centered at ASN19. Cohesin-dockerin linkers C1D1 (PDB ID: 2OZN) and C2D2 (PDB ID: 10HG), were obtained from the PDB webpage and prepared using Amber ff14SB to position Ald6 and Acs1 enzymes on the lipid surface in the proximity of the Atf1 enzyme<sup>47, 48</sup>. In our Brownian Dynamics (BD) simulations, we utilized a lipid monolayer membrane composed of POPC (1-palmitoyl,2-oleoyl-sn-glycerol-3-phosphocholine). As the most abundant phospholipid in animal cell membranes, POPC is widely used in both experimental and simulation studies as a benchmark for phospholipid and bio-membrane research<sup>49-51</sup>. The lipid monolayer surface (420x420 Ų) was generated by placing POPC (1-palmitoyl,2-oleonyl-sn-glycerol-3-phosphocholine) molecules at 8 Å away from each other, resulting in a density of 2.04 x 10<sup>14</sup> cm<sup>2</sup>. The structure and GAFFlipid force-field parameters of a POPC molecule were downloaded from the lipidbook database<sup>52, 53</sup>. The atomic structures of enzymes Ald6, Acs1, and Atf1; linkers C1D1 and C2D2; and the lipid monolayer were then positioned as shown in **Figure 1A** and combined using the AMBER tleap package. The enzymes were strategically positioned to expose their reaction sites to the substrate in the +z direction.

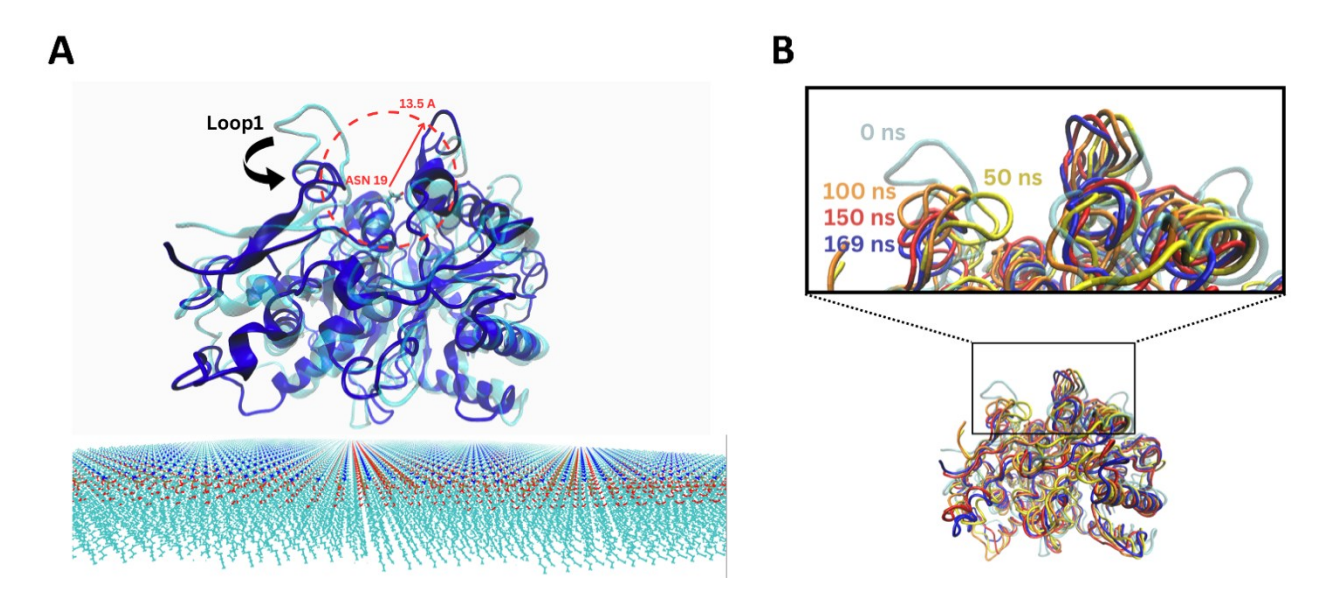


**Figure 2. Selecting Open conformation of Atf1 enzyme.** (A) Structure of Atf1 enzyme. The cyan tube representation shows the initial structure with closed conformation (0 ns), and the blue tube shows the open conformation at 169 ns in a 200 ns aMD trajectory. The red circle indicates the binding site with radius of 13.5Å centered at ASN19 amino acid. (B) Overlay of 5 conformations of Atf1 enzyme shows that the loop region changes from closed to open conformation and has relatively wider opening at 169 ns.

The substrates ACT and ACO were constructed using the open-source Avogadro software and parameterized using General Amber Force Field (GAFF) and AM1-BCC parameters for partial charge calculations<sup>54</sup>. The ionization state of ACO was based on pH 7.5 and had -4e total charge (**Figure 1C**).

# Simulation setup and environmental modeling

*BD* setup. The GeomBD3 program was used for the BD simulations<sup>33</sup>. The prepared multienzyme molecular model and substrates were simulated as all-atom rigid bodies with no internal degrees of freedom. In the BD setups, the test-tube and cell-like environments represent closed and open systems, respectively. The z-direction wall acts as a hard wall in the test-tube setup and as a termination wall in the cell-like environment. The test-tube environment is designed to simulate a controlled, isolated environment with no external influences. In contrast, the cell-like environment allows the system to interact with a larger environment, enabling the exchange of matter. The size of the simulation box for the test-tube environment was 250 Å in the z-direction (perpendicular to the lipid surface) and 420 Å x 420 Å in the x- and y-directions (Figure 1A). A hard boundary was applied at the faces of the box, which resulted in the substrate reverting to its previous position upon crossing the boundary, then a new random component of force was applied to the substrate. To simulate a cell-like environment, the top face (z-direction) of the box was extended to 400 Å and used as a termination wall. When a substrate's replica crossed this wall, it was modeled as a side reaction and terminated, and a new replica was generated from the initial position located in the enzyme active site.

Four models were generated for each step of the reaction, varying the distances between enzymes at d = 60, 80, 100, and 500 Å. For instance, if d=60 Å, then both distances are 60 Å in the model. The measurement of the inter-enzyme distances was taken from the surface of the enzymes (**Figure 1A**). In the setup with a 500 Å inter-enzyme distance, the system was configured with only 2 enzymes between which the reaction occurred, instead of the 3 enzymes. Both enzymes were placed diagonally in opposite corners. This modification aimed to reduce the overall system size and mitigate computational costs.

*BD algorithms*. The program generates 4 grid representations of the simulation box: excluded volume, van der Waals (vdW)-like 12-6 Lennard-Jones potential energy, screened electrostatic potential energy, and desolvation energy. The grid spacing for each type was set at 0.5 Å. The vdW and electrostatic potential grids were extended up to 15 Å and 40 Å, respectively. The electrostatic grid was modeled to represent the implicit monovalent salt concentration of 0.35 M to mimic the experimental conditions. The substrate diffuses in the implicit water-based system according to an overdamped Langevin equation<sup>29</sup>.

$$r_i(t+\Delta t) = r_i(t) - \frac{D_i}{k_B T} \frac{\partial E}{\partial r_i} \Delta t + \sqrt{2D_i \Delta t} \ R$$

where  $D_i$  is the translational or rotational diffusion coefficient,  $k_B$  is the Boltzmann's constant, T is temperature,  $\delta E/\delta r_i$  is the potential gradient computed numerically based on the potential grids,  $\Delta t$  is the time step (0.05 ps in this study), and R is the stationary Gaussian random number with a zero mean.

To speed up BD simulations, each BD run had 100 independent substrate replicas to diffuse from the initial position with different random number seeds, so diffusion of each replica was an independent run from another replica. According to the size of the system, the concentration of ligand was  $37.65 \, \mu M$  considering one substrate molecule in the system. Once the substrate replica was bound to the target enzyme, it was terminated, and a new independent replica was generated from the initial position.

Substrate binding and termination of BD runs. Each BD simulation was terminated when the relative standard deviation of the last 100 average binding time values was less than 3%, with a minimum of 600 successful bindings. To begin a BD replica, substrates ACT and ACO were placed in the binding pocket of Ald6 and Acs1, respectively. The binding criterion is a geometric requirement that requires the ligand to enter inside a certain radius of the active site of the target enzyme. The binding radius for Acs1 and Atf1 was 9.5 Å and 13.5 Å, respectively. The binding spheres with different radii were tested and decided based on the size and molecular shape of the substrate and target enzyme pocket (Supporting Information, Figure S2). In addition, the initial positions for both ligands were selected based on enzyme—ligand interaction and ensured that ACT and ACO could leave Ald6 and Acs1-AMP, respectively, to diffuse away in the system without being stuck in the leaving site (Supporting Information).

## BD simulation outputs and analysis

Format of output files. The GeomBD3 program generates 3 output files for each BD run: a log file, a pqr file, and a dcd file. The simulation log file records the detailed information of association events, which were monitored in real-time. The simulation run was manually terminated when sufficient convergence of average association time was obtained based on its standard deviation. The PQR and DCD files were used for post-analysis with molecular visualization software and Python scripting. From the post-analysis of dcd files, we obtained the bulk diffusion coefficient of the substrate, lipid—substrate interaction energetics, local concentration around the target enzyme, direct bindings, and dwell time.

**Diffusion coefficient and energy calculations.** The 3-D diffusion coefficient values were computed using a section of 100-ns long trajectory where the substrate replicas are freely diffusing without any interaction with the solute or surface. We used Einstein's relation,  $\langle r^2 \rangle = 2$ nDt, where r is the displacement in time t, n is the dimensionality, and D is the diffusion coefficient.

To compute the interaction energetics between the substrate (ACO and ACT) and the lipid surface, we analyzed a specific segment of the continuous trajectory in which the substrate diffused along the lipid surface. The interaction energy calculation includes the 12-6 Lennard-Jones potential for vdW and screened Coulombic potential for electrostatic interactions (Supporting Information). We applied cutoff distances of 12 Å and 40 Å from the surface for vdW and electrostatic interactions, respectively.

Approximation of local substrate concentration. The local concentration of substrate, [S], was computed over a 500-ns trajectory segment within a spherical volume of radius 50 Å surrounding the target enzyme with the following formula:

$$[S] = \frac{\frac{1}{n} \sum_{i=1}^{n} m_i}{V}$$

where n represents the total number of trajectory frames,  $m_i$  the number of substrate replicas present within the spherical shell at the  $i^{th}$  frame, V the volume of the sphere excluding target enzyme, and  $[S_o]$  the bulk substrate concentration across the entire simulation box. The computed values were further converted into  $\mu M$  units, normalized by the bulk concentration,  $[S_o]$ , and denoted as  $[S]/[S_o]$  in the table.

Criteria of direct binding to the target enzyme. Direct bindings have faster kinetics and use shorter binding pathways as compared with indirect bindings. To quantify these bindings, we counted the number of successful trajectories in which a substrate consistently diffuses in proximity to the enzymes within an inner box (Figure 3). The inner box is designed to maintain a minimum 40-Å padded region around the enzyme pairs. This strategic design allowed for specifically counting the successful bindings that occurred without diffusing in the surrounding bath. The size of the inner box varies with the inter-enzyme distances, expanding in the x- and y-dimensions as the distance between enzymes increases. For instance, when the inter-enzyme distance is 60 Å, the inner box accommodates a volume of  $1.6 \times 10^{-15}$  cm<sup>3</sup>. This volume extends to  $1.25 \times 10^{-15}$  cm<sup>3</sup> when the distance between enzymes is 80 Å and further expands to  $1.46 \times 10^{-15}$  cm<sup>3</sup> at 100 Å.

Criteria of computing substrate dwelling time. A substrate may diffuse on the surface of an enzyme before binding, and the amount of time it resides on the surface is called its dwell time. The radius of the dwelling sphere depends on the size of the enzyme and the substrate, allowing a padded region around the enzyme for a substrate to reside (Figure 3). The dwelling spheres for Acs1 and Atf1 have radii of 48 Å and 50 Å, respectively, from the center of mass of the respective enzymes. We recorded the dwell time of the substrate replicas bound in the last 500 ns of each BD run.

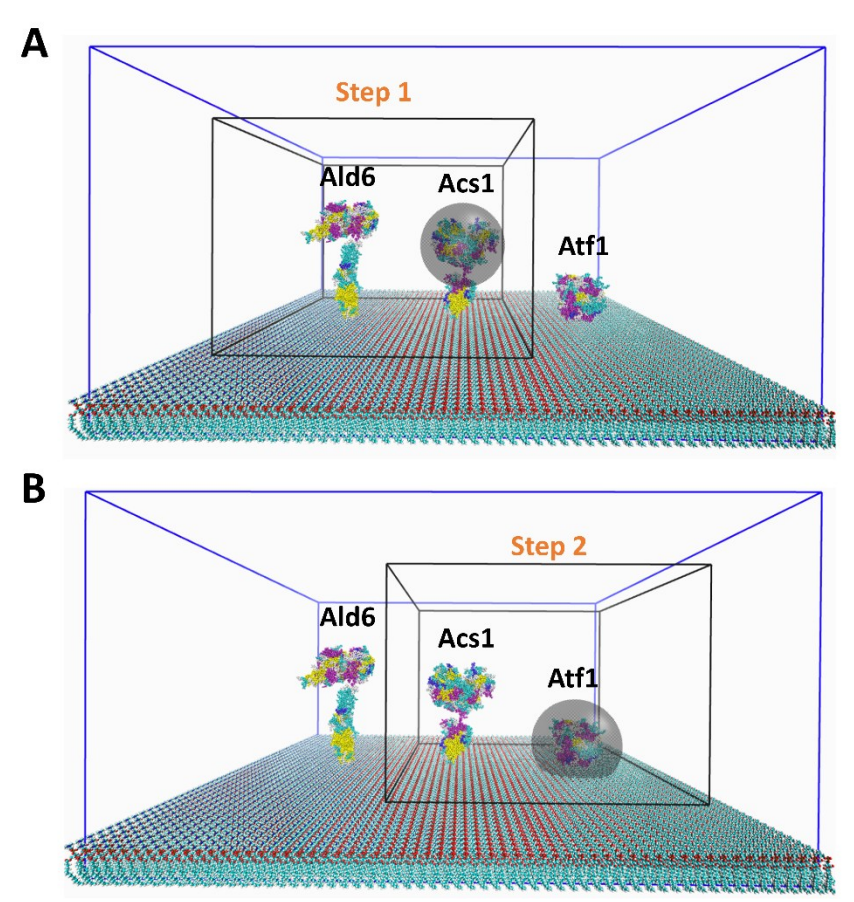


Figure 3. Defining direct-binding cubic box and dwelling sphere for (A) ACT (acetate ion) in step 1, and (B) ACO (acetyl coA) in step 2. The inner black box ensures a minimum of 40-Å padding around the enzymes involved in each reaction step and separates its volume from the surrounding bath. The substrate replicas diffused within the inner box throughout their association event are classified as direct binders. The gray sphere covers the area around the enzyme required for the respective associating substrate to reside on its surface before association. The radii of these dwell spheres are 48 Å and 50 Å for Acs1 and Atf1, respectively, to calculate the dwell time of ACT (acetate ion) in step 1, and ACO (acetyl coA) in step 2.

All files reported in this study are available at <a href="https://github.com/chang-group/GeomBD3/tree/main/Example/folder">https://github.com/chang-group/GeomBD3/tree/main/Example/folder</a> "colocalized yeast-ester biosynthesis enzymes".

#### **RESULTS**

We modeled the yeast-ester biosynthesis process and analyzed the colocalization effect of enzymes on the association rate, local concentration, and diffusion pathways during the process. BD simulations were performed on the 2 steps of the biosynthesis, requiring 2 systems with ACT and ACO ligands, respectively (Figure 1E). In addition to a test-tube-like environment, we included a cell-like environment with side reactions on substrates. Relative enzyme orientations were tested, and the results showed that the orientations did not affect the association pathways for both substrates (Supporting Information). As a result, we selected one relative enzyme orientation shown in the figures in the studies (Figure S3).

## Substrate association in different environments

Before carrying out the production runs, we compared the simulated diffusion coefficients of ACT and ACO substrates with the theoretical values to examine the simulation settings in our BD models. ACT has simulated and theoretical diffusion coefficients of  $7.0\pm0.6 \text{ x } 10^{-6} \text{ cm}^2/\text{s}$  and 19.5 x  $10^{-6} \text{ cm}^2/\text{s}$ , respectively. Similarly, ACO's simulated and theoretical values are  $1.8\pm0.2 \text{ x } 10^{-6} \text{ cm}^2/\text{s}$  and  $3.9 \text{ x } 10^{-6} \text{ cm}^2/\text{s}$ . Because the theoretical approximate of a ligand as a sphere and the environment is not identical (i.e., no salt concentration and enzymes present), identical diffusion coefficients from simulations and theoretical calculations are not anticipated. Nevertheless, the two values are in the ballpark, thus validating the BD setting.

Substrate transportation between enzymes in a closed test-tube environment. When decreasing in inter-enzyme distance from 500 Å to 60 Å in a closed system, the association time of ACT decreased from 8.59 μs to 7.39 μs and ACO from 9.92 μs to 6.70 μs (Figure 4 and Table 1). The reported association time results from the average of 600 independent BD runs for both substrates in their respective systems with different inter-enzyme distances. The Wheeldon group found a 2-fold increase in the rate of both steps using 2 different settings: enzymes placed very far away and enzymes placed with nanometer spacings<sup>40</sup>. The decreased association time from our simulations aligns with the experimental findings.

To further interpret the faster association events when 2 enzymes were placed in close proximity, we hypothesized that the decreasing inter-enzyme distances would result in direct association events of a substrate. Therefore, we analyzed the number of direct associations of both substrates

at different inter-enzyme distances. Only 1% to 2% of the total successful bindings of ACT in Step 1 were direct associations, with none for ACO associations to the third enzyme Atf1 in the second catalytic step (Table 1). Thus, we found no relation between direct association events and colocalization in this system. To address the role of colocalization on direct association and dwell time, we included a run of test tube environment with z = 400 Å (marked as \* in Table 1) to compare with z = 250 Å. Changing the z-axis termination from 250 Å to 400 Å led to an increase in association time for both substrates. This increase is expected due to the decrease in substrate concentration, as association time is inversely dependent on concentration rather than being a constant property like the rate constant. On the other hand, the change in z-axis does not affect the direct association and dwell time which showcases the similar effect of colocalization in both cases having different substrate concentration.

**Table 1.** Association data for ACT and ACO substrates with Acs1 and Atf1 within a closed system (test tube environment) of size  $420 \times 420 \times 250 \text{ Å}^3$ . The bulk concentration of the substrate is  $37.65 \text{ }\mu\text{M}$ , and the salt concentration is 0.35 M.

	Step1; enzyme Acs1; ligand ACT				Step2; enzyme Atf1; ligand ACO					
Inter- enzyme distance	60 Å	60 Å (*)	80 Å	100 Å	500 Å	60 Å	60 Å (*)	80 Å	100 Å	500 Å
Association time, mean ± SD (μs)	7.39 ± 0.08	12.66 ± 0.17	7.68 ± 0.05	7.83 ± 0.04	8.59 ± 0.12	6.70 ± 0.08	8.51 ± 0.19	7.21 ± 0.09	7.69 ± 0.07	9.92 ± 0.06
Total associations	600	600	600	600	600	600	600	600	600	600
Direct associations	12	10	12	8	-	0	0	0	0	-
Average dwell time (ns)	2.00	2.00	2.00	2.00	2.00	6.75	6.75	7.38	7.11	7.5

ACT, acetate ion; ACO, acetyl CoA; \* 400 Å in z direction.

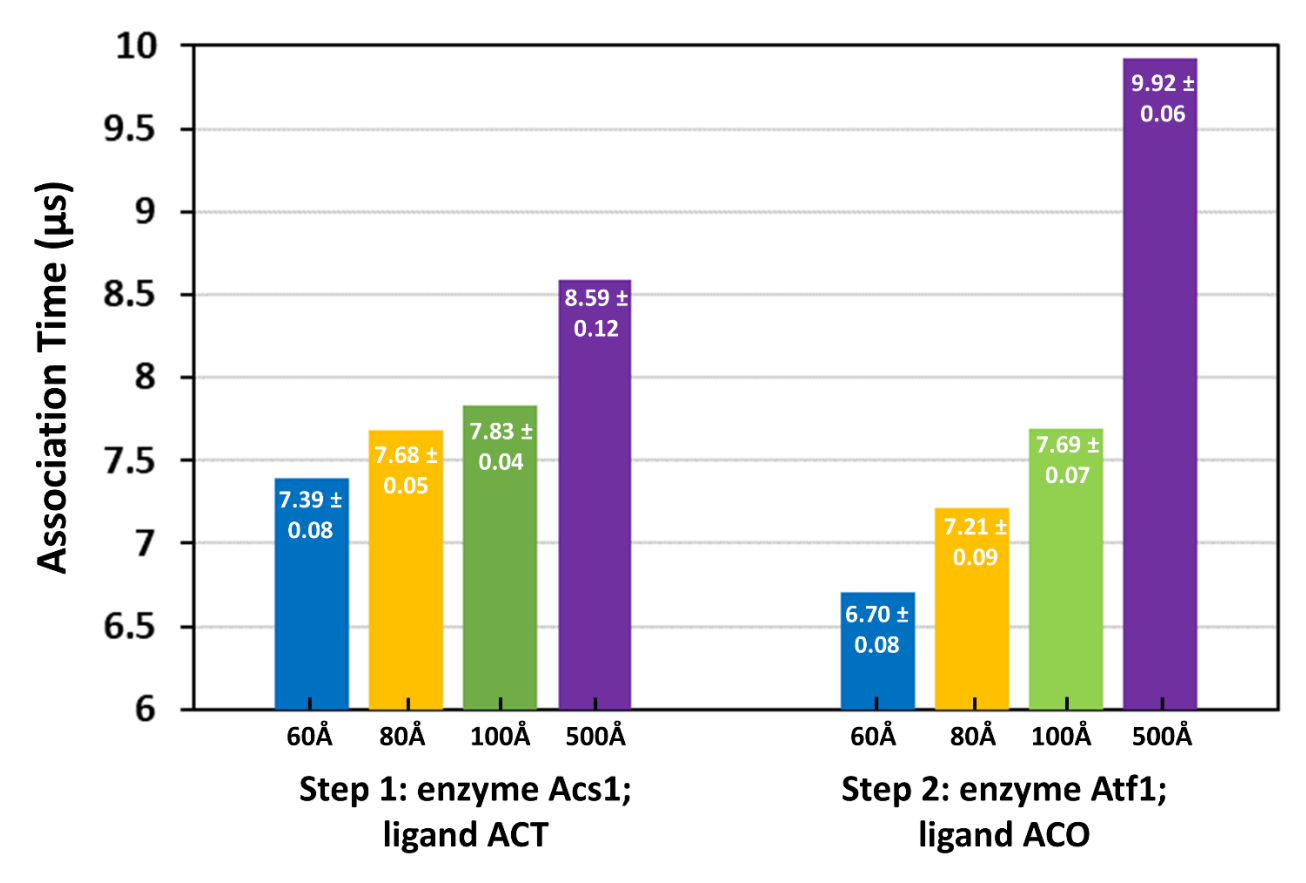


**Figure 4. Relationship between association time and inter-enzyme distance.** Association time of ACT and ACO substrates with Acs1 and Atf1 (step1 and step2) within a closed system (test tube environment) of size 420 x 420 x 250 Å<sup>3</sup>.

Substrate transportation between enzymes in a cell-like environment. In a cell-like environment, a substrate may become catalyzed by a side reaction before encountering its target enzyme, which reduces the total concentration and affects the overall reaction kinetics. Therefore, we assumed that substrates ACT and ACO were metabolized by a side reaction when they reached 400 Å height from the surface (Figure 1A). We chose the systems with 60, 80, and 100 Å inter-enzyme distances for both steps and simulated them under an additional condition of ligand termination in the z-axis at 400 Å.

As shown in **Table 2**, on moving the inter-enzyme distances from 100 Å to 60 Å, the mean substrate ACT association time in Step 1 decreased slightly, from 0.43 µs to 0.37 µs, but the association time was significantly faster than in the test-tube environment. For example, in the

setting of 60 Å inter enzyme distance, the ACT mean association time decreased markedly, from 7.39 µs in the test tube-like environment to 0.37 µs in the cell-like environment. The ACO association time in Step 2 remained unchanged (i.e., ~2.35 µs) in different inter-enzyme distance settings. However, the mean value dropped greatly, from >6.70 in the tube-like environment to 2.35 µs when the side reaction was considered. Moreover, the successful association rate was < 5% in Step 1 and 31% in Step 2. Further investigation of the trajectories revealed that most trajectories that led to successful binding of both substrates were direct associations, with the substrate only diffusing around the enzymes and/or on the surface. Most trajectories showed that the substrate ACT rapidly diffused away from the enzymes and surface, thus losing 95% of the ACT substrate (Table 2). However, ACO is less diffusive and has lower loss probability, thus resulting in higher association time. Here, we can conclude that in a cell-like environment, the side reactions can play a critical role in determining substrate association kinetics.

**Table 2** Average association time and probability of substrate loss in the open system (cell-like environment) for both steps with inter-enzyme distance at 60, 80 and 100 Å.

	Step1; enzyme Acs1; ligand ACT			Step2; enzyme Ald6; ligand ACO			
Inter-enzyme distance	60 Å	80 Å	100 Å	60 Å	80 Å	100 Å	
Association time, mean ± SD (μs)	0.37 ± 0.003	0.42 ± 0.002	0.43 ± 0.002	2.66 ± 0.02	2.53 ± 0.02	2.35 ± 0.01	
Successful binding (%)	4.76	4.31	3.99	31.04	29.95	27.52	
Substrate loss (%)	95.24	95.69	96.01	68.96	70.05	72.48	

ACT, acetate ion; ACO, acetyl CoA

## Effects from the lipid surface on substrate diffusion

Because the surface may offer intermolecular interactions between the lipid and substrate to affect association time and the binding pathway, we calculated the electrostatic ( $E_{elec}$ ) and vdW ( $E_{vdW}$ ) interactions of both substrates with the lipid surface from our BD simulations. Notably, our BD grids used standard all-atom Amber ff14SB and GAFF force fields. As a result, the values were in the ballpark for comparable calculations with atomistic MD simulations. The small and negatively

charged ACT holds close to zero attractions with the surface, with ACT-lipid interaction energies  $\Delta E_{elec}$  and  $\Delta E_{vdW}$  of -0.10  $\pm$  0.07 kcal/mol and -0.08  $\pm$  0.2 kcal/mol, respectively. In contrast, the larger substrate ACO showed increased ligand-lipid interactions, and  $\Delta E_{elec}$  and  $\Delta E_{vdW}$  values were -0.83  $\pm$  0.3 kcal/mol and -1.42  $\pm$  1.02 kcal/mol, respectively. The stronger  $\Delta E_{elec}$  and  $\Delta E_{vdW}$  values may be contributed by the larger size of ACO versus ACT. Furthermore, we compute both  $\Delta E_{elec}$  and  $\Delta E_{vdW}$  between substrates and lipid at various distances (**Figure S4**). We observed that long range electrostatic interactions have minimal contribution to the lipid-substrate interactions. As a result, they do not significantly contribute to the simulations and do not alter the association kinetics (Table S2). BD trajectories of substrate diffusion showed the same trend that ACT quickly diffused far away from the active site, whereas ACO stayed longer around the enzymes and surface.

# Effect from the substrate's local concentration on association kinetics

The substrate's local concentration around the target enzyme plays a vital role in its reactivity. In a kinetic reaction, the substrate's local concentration is directly related to the collision probability and enzyme activity<sup>32</sup>. To further investigate the colocalization effect on local concentration, we calculated the effective concentration of both substrates (ACT and ACO) under the radius of 5 nm from the target enzyme in the systems of different inter-enzyme distances. As shown in **Table 3**, decreasing the inter-enzyme distance increased the local concentration of ACT, which contributed to higher association probability. Of note, the larger substrate ACO held stronger interaction molecular attractions with an enzyme, so the local concentration was not affected by the interenzyme distances. The results suggest that the colocalization of enzymes can increase the local concentration of a substrate around the target enzyme, which helps improve the probability of molecular encounters and thus increases the rate of reaction.

**Table 3**. Local concentration, [S], of ACT and ACO substrates within a 50-Å radius around the enzymes Acs1 and Atf1. The values of [S] are normalized with the bulk concentration,  $[S_o] = 37.65 \, \mu\text{M}$ , and reported as  $[S]/[S_o]$ .

	Step1; en	zyme Acs1;	ligand	Step2; enzyme Atf1; ligand			
	ACT			ACO			
Inter-enzyme	60 Å 80 Å 100 Å			60 Å	80 Å	100 Å	
distance							
[S] (µM)	61.9	56.0	50.1	162.3	150.2	170.2	

$[S]/[S_0]$	1.64	1.49	1.33	4.31	3.99	4.52

ACT, acetate ion; ACO, acetyl CoA

We conjectured that the interactions between the enzyme and substrate could retain the substrate near the protein surface, thereby contributing to increased local concentrations. Therefore, we analyzed the dwelling time of both substrates with their target enzyme. ACT stayed ~2 ns on the surface of its target protein Acs1 (**Table 1**) despite the inter-enzyme distances. ACO had ~6.75 to 7.5 ns of dwell time. Because of its smaller size and weaker intermolecular interactions, ACT had shorter dwell time than ACO. The dwell time remained unchanged with varying inter-enzyme distance, so it does not contribute to the changes in binding kinetics in different enzyme settings.

# **DISCUSSION**

Eukaryotic biochemistry has a defining feature that metabolic pathways can be found in and on membrane-bound organelles. Studies suggested that the spatial organization of the reaction cascade has kinetic advantages in more efficient intermediate transportation<sup>55-58</sup>. Therefore, we hypothesized that colocalization may bring a substrate to associate directly with its target enzyme without diffusing into the bulk solvent. Here, we termed the event "direct association". Because a cell environment exists for various enzymes, we also hypothesized that side reactions occur to an intermediate substrate, thus resulting in losing the substrate for the next catalytic step and reducing the overall product synthesis. Therefore, as compared with a test-tube environment, in cells, direct association such as substrate channeling may be more important. To further understand enzyme colocalization, we modeled substrate associations during the ethyl-acetate biosynthesis pathway in S. cerevisiae. Inter-enzyme distances between 2 enzymes were modeled on lipid droplet membranes to simulate an experimental setup. Notably, although experiments cannot precisely control the inter-enzyme distances, our work allows for computationally placing 2 enzymes separated by a designed distance. Here we chose the distance from 60 Å to 500 Å to mimic colocalization and no colocalization, respectively, in experimental settings. In this work, we focused on substrate transportation and recorded the association time of the substrates ACT and ACO in each chemical step (Tables 1 and 2). We demonstrated that the tube- and cell-like environments significantly affected the average substrate association time.

In a test tube, a substrate can spend an excessively long time diffusing within the water box and eventually diffuse to the active site of the target enzyme. In contrast, in a cell-like environment, a substrate may become catalyzed by a side reaction when it diffuses away from the target enzyme (i.e., reaching 400-Å height from the surface in our BD setting). Therefore, a BD run is terminated, which reduces the average association time. The effect of a side reaction was more pronounced in the smaller substrate ACT, with the average association time being 20 times faster when the side reaction was turned on: ~8 μs in the test-tube environment and ~0.4 μs in the cell-like environment. Of note, ACO was only ~3 times faster in the cell-like environment than in the test-tube environment. The considerable faster association time was due to most (~95%) of ACT being lost during the transportation process, and only those molecules that did not diffuse far away from the enzymes could have successful association. ACT diffused faster than ACO, with simulated diffusion coefficients of  $7.0\pm0.6 \text{ x } 10^{-6} \text{ cm}^2/\text{s}$  and  $1.8.0\pm0.6 \text{ x } 10^{-6} \text{ cm}^2/\text{s}$ , respectively. ACT also had weaker intermolecular interactions with the target enzyme Acs1, which could be quantified by the local substrate concentration: ACT had only ~1.5 times higher local concentration than the bulk substrate concentration as compared with ACO, which had ~4 times increased local concentration (Table 3). Because ACT was lost easily in a cell-like environment, even the average association time and binding probability in colocalization (inter-enzyme distance 60 Å in Table 2) were slightly favorable in binding kinetics, so the contribution in biology can be significant. Different from ACT, the larger substrate ACO had a more non-specific interaction with enzyme Atf1 and ~4.2 times increased local substrate concentration. Even though ~70% of ACO was lost by the side reactions in the cell-like environment, the inter-molecular attractions between Atf1 and the surface played roles to keep more ACO locally.

In contrast to our conjecture, the probability of direct association events was very low, and most of the substrate diffused further than 40 Å away from the surface of either enzyme in the pair (**Figure 3**). Note that although the local substrate concentration was increased, both substrates stayed briefly, 2 to 7.5 ns, on the enzyme surface regardless of the inter-enzyme distances. The effect of local concentration is governed solely by the colocalization of enzymes since the systems of step1 and step2 having different z-axis boundary conditions led to similar number of direct association events and dwell time (**Table 1**). The diffusion was fast; therefore, ACO or ACT could easily diffuse 40 Å away from the enzymes instead, resulting in nearly no direct association events. The only system with the noteworthy percentage of direct association was ACT diffusion to Acs1

when the inter-enzyme distance between Acs1 and Ald6 was 60 Å. Because the lipid surface may provide attractions to keep the intermediate between the 2 enzymes, the membrane may encourage direct association. Moreover, studies also suggest that ligand diffusing in a 2-D surface may increase molecular encounters as compared with diffusing in a 3-D space<sup>59, 60</sup>. The interactions between the lipid and ACT are close to zero, so no 2-D diffusion was observed in ACT. The larger size and negatively charged phosphate groups of ACO yielded stronger vdW (~ -0.8 kcal/mol) and electrostatic (-1.42 kcal/mol) attractions between ACO and the membrane. However, the interactions are not sufficiently strong to hold ACO on the lipid surface for 2-D diffusion. Note that although water and ion molecules were not modeled explicitly, the BD considers desolvation penalty. Although intermolecular interactions help to increase local substrate concentrations and direct binding events to assist substrate association, they cannot be too strong. Overly strong interactions can hamper the product synthesis rate by holding a substrate on a protein or membrane surface. Bioengineering systems may choose a membrane environment to more efficiently keep a substrate in local regions, but the interactions should be moderate.

By using BD to simulate ligand diffusion in different protein arrangements and environment settings, we modeled substrate association time from the enzyme that produces the substrate to the next enzyme in the yeast-ester biosynthetic pathway to investigate enzyme colocalization in both test-tube and cell-like environments. Simply colocalizing a pair of enzymes in proximity on membranes does not provide direct substrate channeling. However, the proximity provides faster substrate association to achieve enhanced overall biosynthesis. Experimental studies showed nearly 2-fold greater ethyl-acetate production rate than in an un-colocalized pathway in a test tube. Our studies suggest that in a cell environment with side reactions to decrease the substrate concentration inside a cell, the overall enhancement of ethyl acetate can be further increased. ~95% of ACT and ~70% of ACO was lost by the side reactions and the leftover faster associating substrate led to the increase in their association time by 20 times and 3 times, respectively. The work explains the factors to achieve more productive final product synthesis in a multi-enzyme cascade and provides insights into the best engineering of enzyme scaffolds to utilize the effects of colocalization of pathway and membrane environment.

# Acknowledgments

This study was supported by the US National Science Foundation (MCB-1932984). Computations were performed using the computer clusters of the University of California, Riverside High Performance Computer Cluster, which were funded by grants from the NSF (MRI-1429826) and the NIH (S10OD016290) and NSF national supercomputer centers ACCESS (CHE130009).

## REFERENCES

- (1) Winkel, B. S. Metabolic channeling in plants. Annu. Rev. Plant Biol. 2004, 55, 85-107.
- (2) Jandt, U.; You, C.; Zhang, Y.-P.; Zeng, A.-P. Compartmentalization and metabolic channeling for multienzymatic biosynthesis: practical strategies and modeling approaches. *Fundamentals and Application of New Bioproduction Systems* **2013**, 41-65.
- (3) Klein, W. P.; Thomsen, R. P.; Turner, K. B.; Walper, S. A.; Vranish, J.; Kjems, J.; Ancona, M. G.; Medintz, I. L. Enhanced catalysis from multienzyme cascades assembled on a DNA origami triangle. *ACS nano* **2019**, *13* (12), 13677-13689.
- (4) Riaz, R.; Ashraf, M.; Hussain, N.; Baqar, Z.; Bilal, M.; Iqbal, H. M. Redesigning robust biocatalysts by engineering enzyme microenvironment and enzyme immobilization. *Catalysis Letters* **2023**, *153* (6), 1587-1601.
- (5) Yi, J.; Li, Z. Artificial multi-enzyme cascades for natural product synthesis. *Current Opinion in Biotechnology* **2022**, *78*, 102831.
- (6) Dunn, M. F. Allosteric regulation of substrate channeling and catalysis in the tryptophan synthase bienzyme complex. *Archives of biochemistry and biophysics* **2012**, *519* (2), 154-166.
- (7) Tran, L.; Broadhurst, R. W.; Tosin, M.; Cavalli, A.; Weissman, K. J. Insights into protein-protein and enzyme-substrate interactions in modular polyketide synthases. *Chemistry & biology* **2010**, *17* (7), 705-716.
- (8) Patel, M.; Korotchkina, L. Regulation of the pyruvate dehydrogenase complex. *Biochemical Society Transactions* **2006**, *34* (2), 217-222.
- (9) Vijayakrishnan, S.; Kelly, S.; Gilbert, R.; Callow, P.; Bhella, D.; Forsyth, T.; Lindsay, J.; Byron, O. Solution structure and characterisation of the human pyruvate dehydrogenase complex core assembly. *Journal of molecular biology* **2010**, *399* (1), 71-93.
- (10) McLain, A. L.; Szweda, P. A.; Szweda, L. I.  $\alpha$ -Ketoglutarate dehydrogenase: a mitochondrial redox sensor. *Free radical research* **2011**, *45* (1), 29-36.
- (11) Bayer, E. A.; Belaich, J.-P.; Shoham, Y.; Lamed, R. The cellulosomes: multienzyme machines for degradation of plant cell wall polysaccharides. *Annu. Rev. Microbiol.* **2004**, *58*, 521-554.
- (12) Kosugi, A. Cellulosomes: plant-cell-wall-degrading enzyme complexes. *Nature reviews microbiology* **2004**, *2* (7), 541-551.
- (13) Dueber, J. E.; Wu, G. C.; Malmirchegini, G. R.; Moon, T. S.; Petzold, C. J.; Ullal, A. V.; Prather, K. L.; Keasling, J. D. Synthetic protein scaffolds provide modular control over metabolic flux. *Nature biotechnology* **2009**, *27* (8), 753-759.
- (14) Moon, T. S.; Dueber, J. E.; Shiue, E.; Prather, K. L. J. Use of modular, synthetic scaffolds for improved production of glucaric acid in engineered E. coli. *Metabolic engineering* **2010**, *12* (3), 298-305.
- (15) Baek, J. M.; Mazumdar, S.; Lee, S. W.; Jung, M. Y.; Lim, J. H.; Seo, S. W.; Jung, G. Y.; Oh, M. K. Butyrate production in engineered Escherichia coli with synthetic scaffolds. *Biotechnology and Bioengineering* **2013**, *110* (10), 2790-2794.

- (16) Bilal, M.; Cui, J.; Iqbal, H. M. Tailoring enzyme microenvironment: State-of-the-art strategy to fulfill the quest for efficient bio-catalysis. *International journal of biological macromolecules* **2019**, *130*, 186-196.
- (17) Armstrong, F. A.; Cheng, B.; Herold, R. A.; Megarity, C. F.; Siritanaratkul, B. From Protein Film Electrochemistry to Nanoconfined Enzyme Cascades and the Electrochemical Leaf. *Chemical Reviews* **2022**, *123* (9), 5421-5458.
- (18) Cao, Y.; Li, X.; Xiong, J.; Wang, L.; Yan, L.-T.; Ge, J. Investigating the origin of high efficiency in confined multienzyme catalysis. *Nanoscale* **2019**, *11* (45), 22108-22117.
- (19) Rocha-Martín, J.; Betancor, L.; López-Gallego, F. Immobilization techniques for the preparation of supported biocatalysts: Making better biocatalysts through protein immobilization. *Biocatalysis for Practitioners: Techniques, Reactions and Applications* **2021**, 63-88.
- (20) Reis, C. L. B.; Sousa, E. Y. A. d.; Serpa, J. d. F.; Oliveira, R. C.; Santos, J. C. S. d. Design of immobilized enzyme biocatalysts: Drawbacks and opportunities. *Química Nova* **2019**, *42*, 768-783.
- (21) Gorfe, A. A.; Chia-en, A. C.; Ivanov, I.; McCammon, J. A. Dynamics of the acetylcholinesterase tetramer. *Biophysical journal* **2008**, *94* (4), 1144-1154.
- (22) Boehr, D. D.; D'Amico, R. N.; O'Rourke, K. F. Engineered control of enzyme structural dynamics and function. *Protein Science* **2018**, *27* (4), 825-838.
- (23) Ghosh, R. K.; Hilario, E.; Chang, C.-e. A.; Mueller, L. J.; Dunn, M. F. Allosteric regulation of substrate channeling: Salmonella typhimurium tryptophan synthase. *Frontiers in Molecular Biosciences* **2022**, *9*, 923042.
- (24) Wheeldon, I.; Minteer, S. D.; Banta, S.; Barton, S. C.; Atanassov, P.; Sigman, M. Substrate channelling as an approach to cascade reactions. *Nature chemistry* **2016**, *8* (4), 299-309.
- (25) Cheng, Y.; Chia-en, A. C.; Yu, Z.; Zhang, Y.; Sun, M.; Leyh, T. S.; Holst, M. J.; McCammon, J. A. Diffusional channeling in the sulfate-activating complex: combined continuum modeling and coarse-grained Brownian dynamics studies. *Biophysical journal* **2008**, *95* (10), 4659-4667.
- (26) Liu, Y.; Matanovic, I.; Hickey, D. P.; Minteer, S. D.; Atanassov, P.; Barton, S. C. Cascade kinetics of an artificial metabolon by molecular dynamics and kinetic Monte Carlo. *ACS Catalysis* **2018**, *8* (8), 7719-7726.
- (27) Nunes-Alves, A.; Kokh, D. B.; Wade, R. C. Recent progress in molecular simulation methods for drug binding kinetics. *Current Opinion in Structural Biology* **2020**, *64*, 126-133.
- (28) Martinotti, C.; Ruiz-Perez, L.; Deplazes, E.; Mancera, R. L. Molecular dynamics simulation of small molecules interacting with biological membranes. *ChemPhysChem* **2020**, *21* (14), 1486-1514.
- (29) Northrup, S. H.; Allison, S. A.; McCammon, J. A. Brownian dynamics simulation of diffusion-influenced bimolecular reactions. *The Journal of Chemical Physics* **1984**, *80* (4), 1517-1524.
- (30) Huber, G. A.; McCammon, J. A. Brownian Dynamics Simulations of Biological Molecules. *Trends Chem* **2019**, *1* (8), 727-738. DOI: 10.1016/j.trechm.2019.07.008.
- (31) Muñiz-Chicharro, A.; Votapka, L. W.; Amaro, R. E.; Wade, R. C. Brownian dynamics simulations of biomolecular diffusional association processes. *Wiley Interdisciplinary Reviews: Computational Molecular Science* **2023**, *13* (3), e1649.
- (32) Hong, X.; Cholko, T.; Chia-en, A. C.; Wheeldon, I. Multiscale simulation-guided design of enzyme bioconjugates with enhanced catalysis. *Chem Catalysis* **2022**, *2* (10), 2691-2703.
- (33) Cholko, T.; Kaushik, S.; Wu, K. Y.; Montes, R.; Chang, C.-e. A. GeomBD3: Brownian dynamics simulation software for biological and engineered systems. *Journal of chemical information and modeling* **2022**, *62* (10), 2257-2263.
- (34) Bruce, N. J.; Ganotra, G. K.; Richter, S.; Wade, R. C. KBbox: A toolbox of computational methods for studying the kinetics of molecular binding. *Journal of chemical information and modeling* **2019**, *59* (9), 3630-3634.

- (35) Idan, O.; Hess, H. Origins of activity enhancement in enzyme cascades on scaffolds. *ACS nano* **2013**, 7 (10), 8658-8665.
- (36) Lin, Y.-C.; Kim, W. K.; Dzubiella, J. Coverage fluctuations and correlations in nanoparticle-catalyzed diffusion-influenced bimolecular reactions. *The Journal of Physical Chemistry C* **2020**, *124* (44), 24204-24214.
- (37) Huang, Y. m. M.; Huber, G. A.; Wang, N.; Minteer, S. D.; McCammon, J. A. Brownian dynamic study of an enzyme metabolon in the TCA cycle: Substrate kinetics and channeling. *Protein Science* **2018**, *27* (2), 463-471.
- (38) Elcock, A. H.; Huber, G. A.; McCammon, J. A. Electrostatic channeling of substrates between enzyme active sites: comparison of simulation and experiment. *Biochemistry* **1997**, *36* (51), 16049-16058.
- (39) Elcock, A. H. Atomistic simulations of competition between substrates binding to an enzyme. *Biophysical journal* **2002**, *82* (5), 2326-2332.
- (40) Lin, J.-L.; Zhu, J.; Wheeldon, I. Synthetic protein scaffolds for biosynthetic pathway colocalization on lipid droplet membranes. *ACS Synthetic Biology* **2017**, *6* (8), 1534-1544.
- (41) Biasini, M.; Bienert, S.; Waterhouse, A.; Arnold, K.; Studer, G.; Schmidt, T.; Kiefer, F.; Cassarino, T. G.; Bertoni, M.; Bordoli, L. SWISS-MODEL: modelling protein tertiary and quaternary structure using evolutionary information. *Nucleic acids research* **2014**, *42* (W1), W252-W258.
- (42) Meaden, P. G.; Dickinson, F. M.; Mifsud, A.; Tessier, W.; Westwater, J.; Bussey, H.; Midgley, M. The ALD6 gene of Saccharomyces cerevisiae encodes a cytosolic, Mg2+-activated acetaldehyde dehydrogenase. *Yeast* **1997**, *13* (14), 1319-1327.
- (43) Fujii, T.; Nagasawa, N.; Iwamatsu, A.; Bogaki, T.; Tamai, Y.; Hamachi, M. Molecular cloning, sequence analysis, and expression of the yeast alcohol acetyltransferase gene. *Applied and environmental microbiology* **1994**, *60* (8), 2786-2792.
- (44) Jogl, G.; Tong, L. Crystal structure of yeast acetyl-coenzyme A synthetase in complex with AMP. *Biochemistry* **2004**, *43* (6), 1425-1431.
- (45) Case, D.; Ben-Shalom, I.; Brozell, S.; Cerutti, D.; Cheatham III, T.; Cruzeiro, V.; Darden, T.; Duke, R.; Ghoreishi, D.; Gilson, M. AMBER 2018; 2018. *University of California, San Francisco* **2018**.
- (46) Hamelberg, D.; Mongan, J.; McCammon, J. A. Accelerated molecular dynamics: a promising and efficient simulation method for biomolecules. *The Journal of chemical physics* **2004**, *120* (24), 11919-11929.
- (47) Carvalho, A. L.; Dias, F. M.; Prates, J. A.; Nagy, T.; Gilbert, H. J.; Davies, G. J.; Ferreira, L. M.; Romão, M. J.; Fontes, C. M. Cellulosome assembly revealed by the crystal structure of the cohesin–dockerin complex. *Proceedings of the National Academy of Sciences* **2003**, *100* (24), 13809-13814.
- (48) Adams, J. J.; Gregg, K.; Bayer, E. A.; Boraston, A. B.; Smith, S. P. Structural basis of Clostridium perfringens toxin complex formation. *Proceedings of the National Academy of Sciences* **2008**, *105* (34), 12194-12199.
- (49) Kučerka, N.; Tristram-Nagle, S.; Nagle, J. F. Structure of fully hydrated fluid phase lipid bilayers with monounsaturated chains. *The Journal of membrane biology* **2006**, *208*, 193-202.
- (50) Leekumjorn, S.; Sum, A. K. Molecular characterization of gel and liquid-crystalline structures of fully hydrated POPC and POPE bilayers. *The Journal of Physical Chemistry B* **2007**, *111* (21), 6026-6033.
- (51) Benedetto, A.; Bingham, R. J.; Ballone, P. Structure and dynamics of POPC bilayers in water solutions of room temperature ionic liquids. *The Journal of chemical physics* **2015**, *142* (12).
- (52) Domański, J.; Stansfeld, P. J.; Sansom, M. S.; Beckstein, O. Lipidbook: a public repository for force-field parameters used in membrane simulations. *The Journal of membrane biology* **2010**, *236* (3), 255-258.
- (53) Dickson, C. J.; Rosso, L.; Betz, R. M.; Walker, R. C.; Gould, I. R. GAFFlipid: a General Amber Force Field for the accurate molecular dynamics simulation of phospholipid. *Soft Matter* **2012**, *8* (37), 9617-9627.

- (54) Wang, J.; Wolf, R. M.; Caldwell, J. W.; Kollman, P. A.; Case, D. A. Development and testing of a general amber force field. *Journal of computational chemistry* **2004**, *25* (9), 1157-1174.
- (55) Zhang, Y.; Hess, H. Toward rational design of high-efficiency enzyme cascades. ACS Publications: 2017; Vol. 7, pp 6018-6027.
- (56) Rabe, K. S.; Müller, J.; Skoupi, M.; Niemeyer, C. M. Cascades in compartments: En route to machine-assisted biotechnology. *Angewandte Chemie International Edition* **2017**, *56* (44), 13574-13589.
- (57) Vázquez-González, M.; Wang, C.; Willner, I. Biocatalytic cascades operating on macromolecular scaffolds and in confined environments. *Nature Catalysis* **2020**, *3* (3), 256-273.
- (58) Man, T.; Xu, C.; Liu, X.-Y.; Li, D.; Tsung, C.-K.; Pei, H.; Wan, Y.; Li, L. Hierarchically encapsulating enzymes with multi-shelled metal-organic frameworks for tandem biocatalytic reactions. *Nature Communications* **2022**, *13* (1), 305.
- (59) Cholko, T.; Chang, C.-e. A. Modeling Effects of Surface Properties and Probe Density for Nanoscale Biosensor Design: A Case Study of DNA Hybridization near Surfaces. *The Journal of Physical Chemistry B* **2021**, *125* (7), 1746-1754.
- (60) Roberts, C. C.; Chang, C.-e. A. Modeling of enhanced catalysis in multienzyme nanostructures: effect of molecular scaffolds, spatial organization, and concentration. *Journal of chemical theory and computation* **2015**, *11* (1), 286-292.